LATTICE DESIGN OF THE 144 MEV INDUCTION MICROTRON FOR C-60*

Taufik[1†], T. Adachi[1], The Graduate University of Advanced Studies, Tsukuba, Japan
[1]also at High Energy Accelerator Research Organization, Accelerator Laboratory, Tsukuba, Japan
M. Wake, K. Takayama, High Energy Accelerator Research Organization, Accelerator Laboratory,
Tsukuba, Japan

Abstract

A recently proposed racetrack-shape fixed field induction accelerator [1] has been more specifically refined as the 144 MeV Induction Microtron for C-60. Two approaches of tracking simulation taking 3D magnetic fields of a 90 degree bending magnet into account and linear optics calculation have been developed for refining design. It turned out that an inherent feature originated from a finite magnet length and the incidence/exit angle of 45 degree produces a kind of systematic closed orbit distortion depending on particle energy. Orbit stability in the horizontal direction can be achieved by introducing steering magnets or improving the magnetic field homogeneity in the Z direction. Dispersion function of another important lattice function is analytically evaluated and compared with the result obtained through the 3D beam tracking.

INTRODUCTION

Since successful demonstrations of the induction synchrotron concept using the KEK proton synchrotron facility in 2007 [2] and 2013[3], acceleration of giant cluster ions such as C-60 or Si-100 in circular induction accelerators has become realistic. One of such accelerators is an induction microtron (IM) or racetrack-shape fixed field induction accelerator (RAFFIA), which was proposed in 2015[1]. The basic IM lattice consists of four fixed field bending magnets with a reversed field strip at its front edge and field gradient on the main pole face and focusing doublet Qs as seen in Figs. 1 and 2. Two straight sections are occupied by these doublets, injection/extraction devices, and induction acceleration cells.

Concept of betatron motion during a limited time period (or instantaneously) stands even in the IM. The lattice functions such as beta-function or momentum dispersion function can be defined. It is well-known that the closed orbit distortion (COD) takes a crucial role when discussing the orbit stability in a synchrotron. This is true even in the IM. Imperfections in guiding magnetic fields are inevitable in general. Some of them is a major source of the COD. When the COD of a beam centroid orbit exceeds a tolerable level, the IM never works as an accelerator.

Beam dynamics in the IM may be characterized by an inherent feature of the non-uniformity in the bending field along the beam orbit. The orbit in the bending magnet largely varies with energy, as shown in Fig. 1. The feature

is distinguished from the property of a synchrotron. There is the so-called fringing field in a synchrotron bending magnet, which is originated from its finite physical size. However, it does not become a source of the COD in a synchrotron with the same beam orbit from injection to end of the acceleration, because the fringing effects are simply normalized in the term of effective length of magnet. Unfortunately it is not the case in the IM, where the orbit propagates in the different physical region with acceleration. The non-homogeneity of magnetic field along the Z-direction shown in Fig. 1 becomes a source of the COD, varying with energy. It is noted that this error is systematic and generates the intrinsic COD. If an infinitely long magnet is employed, this problem should disappear. As a matter of fact, its physical size is determined from its cost and available accelerator space. We have to compromise more or less, resulting in a notable and intrinsic COD.

It is quite important to estimate the intrinsic COD as well as other lattice functions and establish how to correct the intrinsic COD at the stage of design. Two approaches that have been developed for this purpose are discussed. It is shown that both approaches are useful to optimize the IM lattice and orbit correction.

SCHEMATIC LATTICE

The configuration of the IM is shown in Fig. 1. Steering magnets, the necessity of which will be explained soon, are symmetrically placed on two straight sections. Cluster ions delivered from the ion source are injected into the IM by the injection kicker. After the beams energy achieves extraction energy, ions are extracted by a specific extraction system not shown here.
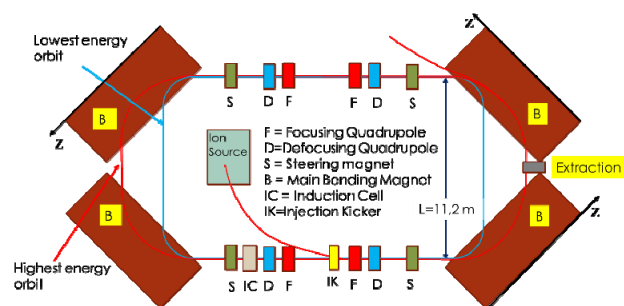

Figure 1: Schematic view of the IM.

BEAM AND MACHINE PARAMETERS

C-60 (A=720, Z = 10) is assumed through the paper. Injection energy and extraction energy are assumed to be

10 MeV and 144 MeV, respectively. The distance between two common trajectories (L) is 11.2 m. The field profile of an ideal bending magnet is shown in Fig. 2 and uniform in the Z direction, which is characterized by constant reverse field and gradient field of 0.079823 T/m.
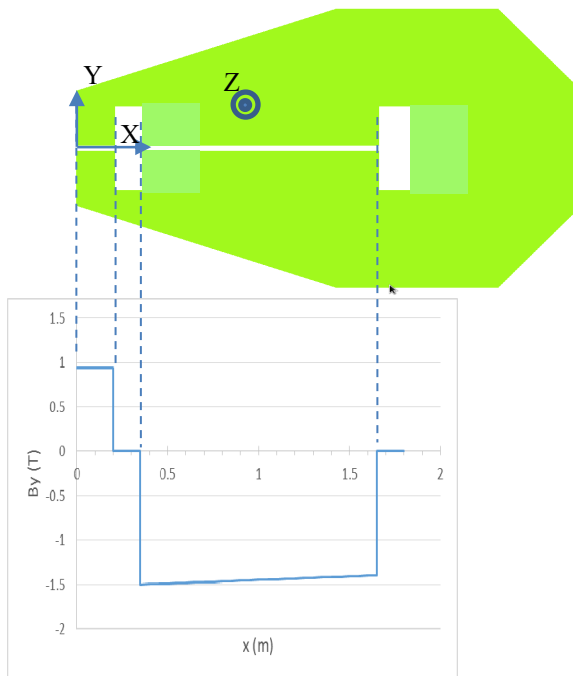

Figure 2: Ideal magnetic field of the bending magnet.

LINEAR BEAM OPTICS THEORY

Lattice Function

Ions perform their own betatron oscillations after injection. Size of the oscillation amplitude is crucial. It is simply written in a term of $(\varepsilon\beta)^{1/2}$ where ε is an emittance and β is the beta-function. The beta-function is straightforwardly determined from the focusing components. To simply obtain the beta-functions of the IM, the four-fold symmetry of the lattice is assumed. One quadrant of the IM lattice consists of drift space on the straight section, focusing quadrupole, defocusing quadrupole, bending magnet, and the other drift space, as shown in Fig. 3. Its optics components are described in the horizon-
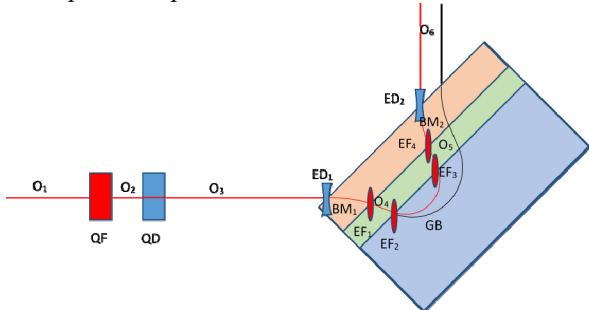

Figure 3: One quadrant of the lattice of RAFFIA.

tal direction. In the vertical direction, the optic component is opposite to that of the horizontal direction except for

the bending magnet. The lattice in the bending magnet region divides into 3 regions, reversed flat bending magnet (BM), drift space (O) and normal bend with field gradient (GB). Edge focusing/defocusing is given as a thin lens. It depends on the entrance beam angle to the magnet edge.

Beta-function can be calculated by finding the transfer matrix along the lattice. The transfer matrix of each component of the IM except for the normal bend region with field gradient is known. On the contrast, the transfer matrix in the bending magnet can be obtained by solving numerically the betatron equation Eq. (1)[1].

$$x'' + \left[\frac{1}{\rho^2(s)} + k(s)\right]x = 0$$
$$y''(s) - k(s)y = 0 \tag{1}$$
$$k(s) = -\frac{1}{B\rho}\frac{\partial B_y(s)}{\partial x}$$

For injection and extraction energy, the transfer matrix in the bending magnet is resumed in Table 1.

Table 1: Transfer Matrix in the Gradient Region of Bending Magnet

Particle Energy	Horizontal (x)		Vertical (y)	
10 MeV	$\begin{pmatrix} -0.352 & 0.793 \\ -1.104 & -0.352 \end{pmatrix}$		$\begin{pmatrix} 0.928 & 1.582 \\ -0.088 & 0.928 \end{pmatrix}$	
144 MeV	$\begin{pmatrix} 0.026 & 3.547 \\ -0.282 & 0.0264 \end{pmatrix}$		$\begin{pmatrix} 0.785 & 4.989 \\ -0.077 & 0.785 \end{pmatrix}$	

The total transfer matrix (M) of the IM is obtained by multiplying all of the transfer matrices sequentially; then, the transfer matrix M must satisfy the stable condition

$$\left|\frac{Trace(M)}{2}\right| \leq 1. \tag{2}$$

Since the bending magnet field is fixed, the k-value of the focusing quadrupole (KF) and defocusing quadrupole (KD) must be determined so that the transfer matrix M satisfies Eq. (2) through the entire accelerating energy. Eq. (2) immediately gives the stability region for KF and KD, Such stability regions at injection energy are shown in Fig. 4.
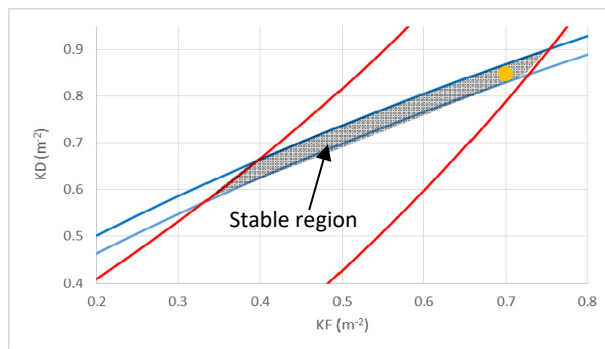

Figure 4: The stability region in the KF-KD space at injection energy.

When KF of 0.7 m^{-2} and KD of 0.85 m^{-2} are for injection energy and 0.8 m^{-2} and 0.92 m^{-2} for extraction energy are chosen, the realized horizontal beta-function for the half lattice of the IM is showed in Fig. 5.
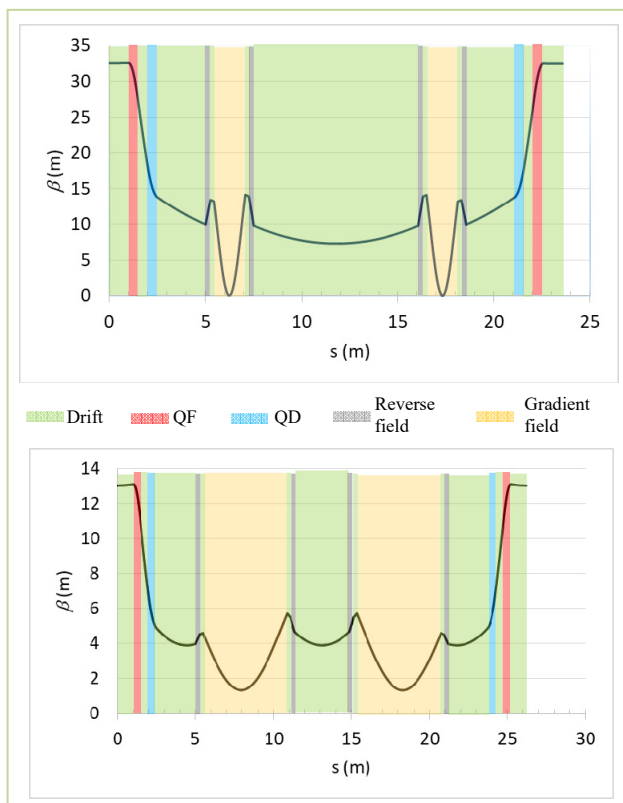

Figure 5: Beta-function in the horizontal direction at injection (upper) and extraction energy (lower).

Closed Orbit Distortion

As a matter of fact, it is difficult to realize an ideal magnetic field profile because of a finite physical size of the magnet. As a consequence of this magnetic field error $\Delta B_y(s)$ that is deviation from the ideal field, the COD caused by $\Delta B_y(s)$ is described in the following equation:

$$X_{COD}(s) = \frac{\sqrt{\beta(s)}}{2\sin(\mu/2)} \int_s^{s+C} \left\{ \frac{\Delta B_y(s')}{B\rho} \right\} \sqrt{\beta(s')} \cos\left[\mu/2 - |\Psi(s) - \Psi(s')| \right] ds'$$
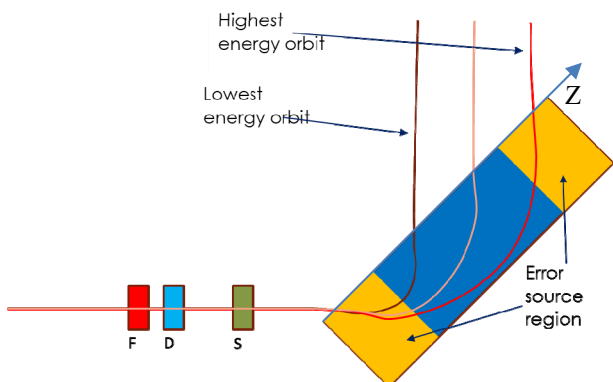
$$(3)$$

Figure 6: Beam orbits and bending maget with field shoulder in the Z direction.

Non-uniformity of The Bending Felds and ΔBy(s)
Non-uniformity in the magnetic field exists as a function of Z that is the mechanical coordinate of magnet in Fig. 1. In general the field profile falls toward the magnet edge without shimming. Thus, $\Delta B_y(s)$ depends on the particle energy, as illustrated in Fig. 6. There it is shown that a low and high energy particle leave from the uniform field region and the other field shoulder region, respectively, although they enter into the same field shoulder region.

The IM bending magnet has been designed using the 3D field calculation software, ACCSIM. Although its design has not been finalized yet, it has been designed so that the field shoulder is minimized. $\Delta B_y(s)$ should be reduced. The magnetic field of the designed bending magnet along the Z coordinate at a certain X position is given in Fig. 7, where a slight non-uniformity in the center region and steep shoulder in both edge are observable.
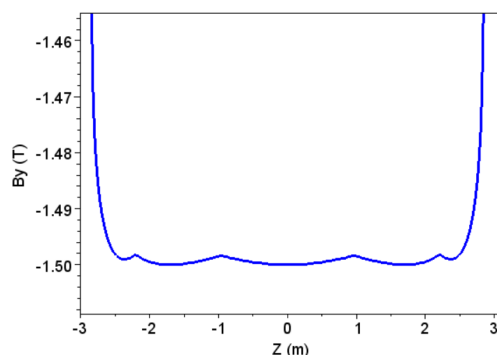

Figure 7: Magnetic field ($B_y(Z)$) of the designed IM bending magnet at X=1.7 m.

COD Calculation Once the orbit is determined assuming the ideal bending fields as shown in Fig. 2 and the realistic $B_y(X,Z)$ is fixed, the deviation from B_y (X,0), $\Delta B_y(s)$ is evaluated. Substituting this $\Delta B_y(s)$ into Eq. (3), we have the COD. The CODs at injection and extraction energy are shown in Fig. 8. The field error source $\Delta B_y(s)$ at extraction energy is much larger than at injection energy. However, the higher magnet rigidity ($B \cdot \rho$) leads to the smaller COD at extraction energy.

COD Correction The COD can be reduced by the steering magnets that are placed at the symmetric positions and excited at the time varying but same current. By adjusting excitation current in time, the corrected COD for injection and extraction energy are obtained respectively at steering field -0.019 Tesla·m and 0.051 Tesla·m.
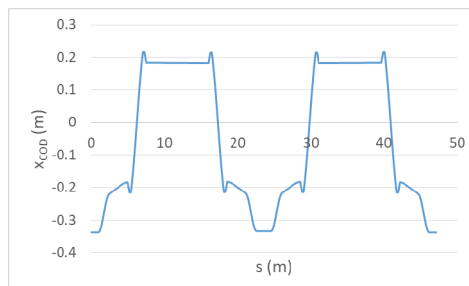
(a)
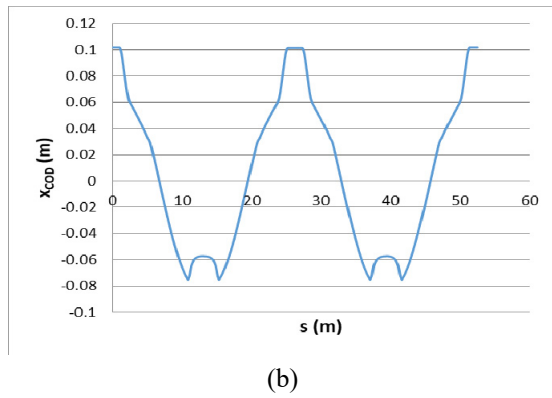
(b)

Figure 8: (a) COD at injection energy and (b) COD at extraction energy.

Dispersion Function

Size of the equilibrium orbit $x_{eq}(s)$ originated from momentum deviation is also important as well as the COD. It is expressed in the following formula similar to that of the COD.

$$D(s) = \frac{\sqrt{\beta(s)}}{2\sin(\mu/2)} \int_s^{s+C} \left(\frac{1}{\rho(s')}\right) \sqrt{\beta(s')} \cos\left[\mu/2 - |\Psi(s) - \Psi(s')|\right] ds' \quad (4)$$

where $D(s) = x_{eq}(s)/(\Delta p/p)$ is the dispersion is function and ρ is the bending radius curve along the orbit of the particle where negative comes from the reverse field region and the positive one comes from the gradient field region of bending magnet.

The dispersion function of the microtron at the extraction energy is given in Fig. 9. Assuming $\Delta p/p$ = 0.5 % and the maximum D of 3.6 m seen in Fig. 9, the maximum x_{eq} is around 1.8 mm. It is sufficiently small. The dispersion function in the straight section where induction accelerator devices are placed is zero. This suggests, there is no emittance blow-up caused by synchro-beta coupling[4].
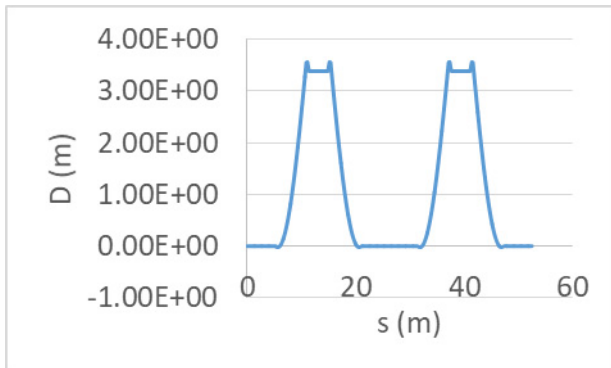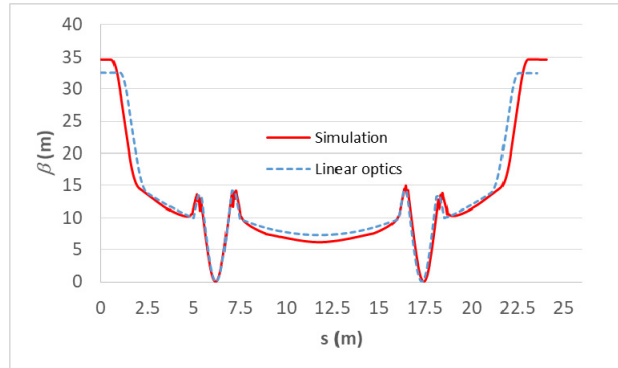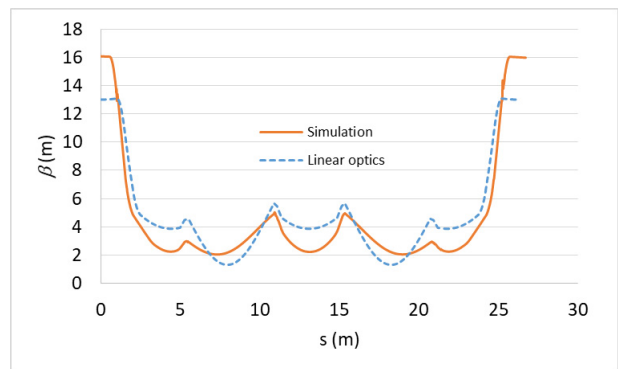

Figure 9: Dispersion function at 144 MeV energy.

COMPARISON WITH 3D BEAM TRACK-ING RESULTS

Lattice Function

The COD and dispersion function evaluated from the linear theory are compared with the results obtained by extensive 3D-beam tracking simulations. With respect to the lattice functions, both approaches seem to be in a good agreement. Fig. 10 shows that the comparison of both approaches for beta-function and dispersion function is very close to each other.
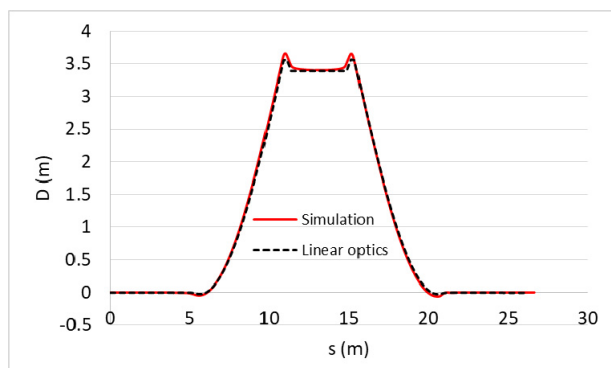

(a)

(b)
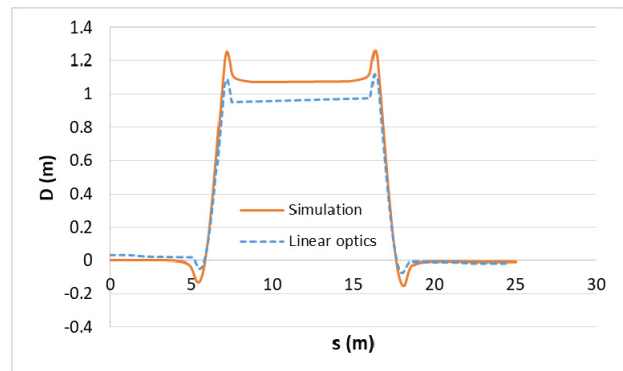
(c)

(d)

Figure 10: Comparison with beam tracking simulation; (a) Beta function at 10 MeV, (b) Beta function at 144 MeV, (c) Dispersion function at 10 MeV and (d) Dispersion function at 144 MeV.

COD

The CODs obtained by both approaches are shown in Fig. 11 (a) and (b). Both approaches achieve almost same COD at injection energy. Meanwhile, a big difference is found for 144 MeV. This discrepancy is attributed to a difference of $\Delta B(s)$ that has been assumed in the calculations, as shown in Fig. 12. In the multi-particle tracking simulation, the orbit is calculated under the entire magnetic field distribution including the fringing fields of magnet. At 144 MeV, the ions orbit enters deeply into the non-uniform field region of the bending magnet. A small orbit difference seems to result in a significant $\Delta B_y(s)$ in the non-uniform field region.
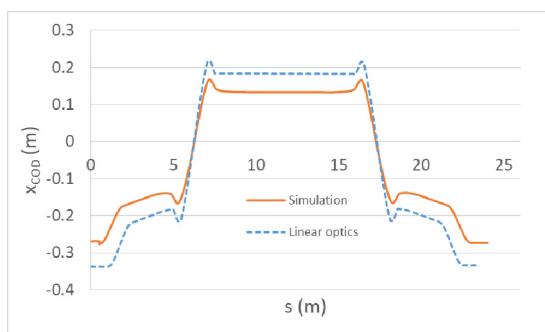
(a)
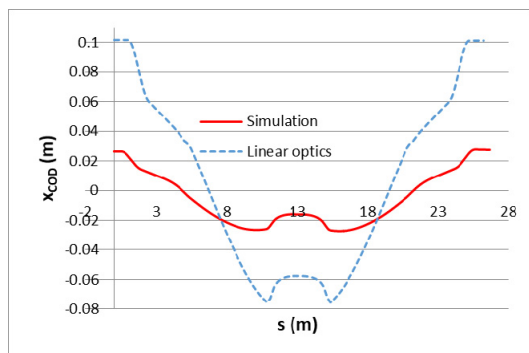
(b)

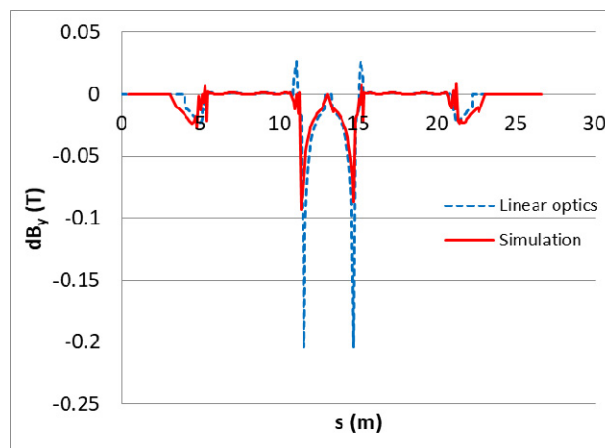Figure 11: Comparison with beam tracking simulation; (a) COD at 10 MeV, (b) COD at 144 MeV.

Figure 12: Comparison with beam tracking simulation of $\Delta B_y(s)$ at 144 MeV.

CONCLUSION

The field non-uniformity in the bending magnet of the IM becomes a systematic field error that varies with the particle energy. This systematic field error generates a inherent COD. Additional magnetic field of steering magnets is required to minimize the COD. It is noted that the correction fields must be changed associated with energy increase. Improving the magnetic field homogeneity in the Z direction is also possible way to reduce the COD by optimization of the pole shape of the magnet. It turned out that the size of equilibrium orbit is still tolerable.

ACKNOWLEDGEMENT

REFERENCES

[1] K.Takayama *et al.*, "A Racetrack-shape Fixed Field Induction Accelerator for Giant Cluster Ions", *Phys. Rev. ST Accel Beams,* vol. 18, p. 050101, 2015.

[2] K.Takayama *et al.*, "Experimental Demonstration of the Induction Synchrotron", Phys. Rev. Lett., vol. 98, p. 054801-4, Feb.2007.

[3] K.Takayama *et al.*, "Induction Acceleration of Heavy Ions in the KEK Digital Accelerator: Demonstration of a Fast-Cycling Induction Synchrotron", Phys. Rev. ST Accel Beams, vol. 17, p. 010101, 2014

[4] T. Monma *et al.*, "Coherent Synchro-Beta Coupling in the KEK Digital Accelerator", Proc. of HIAT2015, MO-PA16 (2016)